ORGANOMETALLICS

pubs.acs.org/Organometallics Article

Scope and Mechanism of the Ruthenium-Catalyzed Deaminative Coupling Reaction of Enones with Amines via Regioselective C_α−C_β Bond Cleavage

Dulanjali S. Thennakoon, Marat R. Talipov,* and Chae S. Yi*

Cite This: *Organometallics* 2023, 42, 2867−2880 Read Online

ACCESS | Metrics & More | Article Recommendations | Supporting Information

ABSTRACT: A highly regioselective C−C bond cleavage method of enones has been devised from the ruthenium-catalyzed deaminative coupling reaction with simple amines. The analogous catalytic coupling reaction of enones with anilines has led to a regioselective C_α−C_β bond cleavage of enones in forming *N*-alkylanilines and 2,4-disubstituted quinolines. The reaction profile study showed the formation of a β-aminoimine intermediate prior to the C−C cleavage product formation. A Hammett plot from the reaction of (*E*)-2-octen-4-one with a series of *para*-substituted benzylamines established a strong promotional effect by an electron-donating group (ρ = −0.77 ± 0.1). The most significant carbon kinetic isotope effect was observed on the α-carbon of the product (C_α = 1.018). The DFT calculations revealed a detailed mechanism of the coupling reaction via consecutive C−H activation and C−C cleavage steps, followed by enamine-to-imine rearrangement and hydrolysis steps. The catalytic method combines hydrogen borrowing and deaminative coupling strategies to furnish a general C_α−C_β bond cleavage protocol for enones.

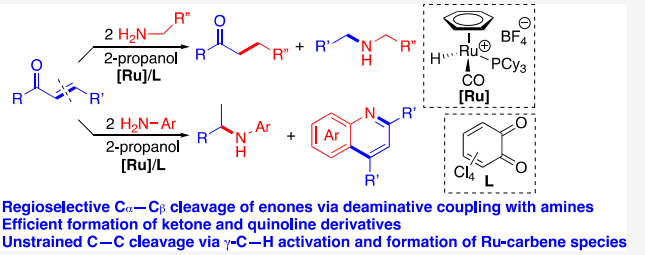

INTRODUCTION

Designing selective C−C bond activation methods for unstrained hydrocarbon compounds constitutes one of the paramount challenges in catalysis research that has profound implications in both the development of sustainable synthetic protocols as well as for reforming biomass and petroleum feedstocks.[1] Since heterogeneous C−C bond cleavage processes are inherently energy intensive and are often unsuitable for fine chemical synthesis,[2] much research effort has been devoted to develop selective C−C bond activation methods by using soluble transition metal catalysts. Early on, cyclopropanes and strained cyclic compounds have been found to be versatile substrates for a variety of catalytic C−C bond activation and insertion reactions where a release of ring strain energy has been exploited for the synthesis of complex organic molecules.[3] In sharp contrast, catalytic C−C bond activation methods for unstrained hydrocarbon substrates have been rarely utilized in the organic synthesis of natural products and pharmacological agents.

Since Milstein's pioneering report on arene $C(sp^2)$−CH_3 bond activation reaction in forming a Rh-PCP pincer complex (Scheme 1A),[4] a number of innovative catalytic strategies have been devised to promote regioselective C−C bond activation and functionalization reactions of unreactive hydrocarbon substrates.[5] Chelate assistance strategy has been proven to be particularly effective for mediating regioselective carbonyl CO−C bond activation reactions of unstrained ketones (Scheme 1B).[6] Catalytic β-carbon elimination and *retro*-allylation methods have been shown to promote regioselective C−C bond cleavage reactions for a variety of saturated and unsaturated hydrocarbon substrates bearing a heteroatom functional group.[7] Catalytic C−C cleavage methods for nitriles and carboxylic acid derivatives as well as alcohols have been successfully utilized for a variety of C−C and carbon-heteroatom bond forming reactions.[5,8] Catalytic C−C cleavage reactions of unstrained hydrocarbon substrates have also been achieved by harnessing the aromatization energy, as exemplified by recent reports on synthesis of arene-containing products.[9] In a seminal work, Dong and co-workers devised Ir-catalyzed deacylative CO−C bond activation and trans-formation method of ketones, which is driven by the formation of heteroarenes (Scheme 1C).[10] Dong group also reported a series of catalytic "cut-*n*-sew" C−C bond insertion methods that are driven by a relief of ring strain and are accompanied by insertion reactions.[11] Lautens and co-workers reported an efficient synthesis of *spiro*-fused benzocyclobutene derivatives by merging remote C−H functionalization and β-carbon elimination protocols.[12] A number of photoredox-catalytic C−C bond cleavage methods have been achieved mainly for the

Received: July 19, 2023
Published: August 21, 2023

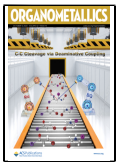

Scheme 1. Transition-Metal-Mediated Unstrained C−C Bond Activation Methods

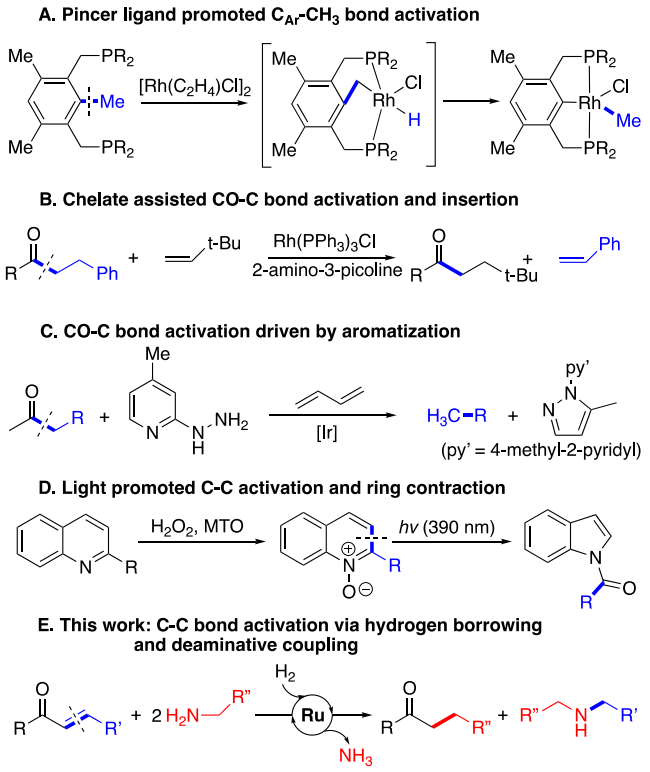

hydrocarbon substrates bearing a heteroatom functional group to form a diverse array of molecular scaffolds.[13] Notably, Levin and co-workers devised a uniquely selective photocatalytic C−C bond cleavage and ring contraction reaction of quinoline *N*-oxides to *N*-acylindoles (Scheme 1D).[14] Despite such remarkable advances, the development of catalytic C(sp^3)−C(sp^3) bond activation and functionalization methods for unstrained aliphatic compounds still remains as a challenging goal, as most of the current technologies either employ strained and activated substrates or are limited to C(sp^2)−C(sp^2) and C(sp^2)−C(sp^3) activation of unsaturated hydrocarbon substrates.[3,9,15]

Inspired by seminal reports on chelate-assisted C−C bond activation strategy,[6] we have been searching for suitable coupling partners that would serve as a chelate directing group for promoting the regioselective C−C bond activation reaction of unstrained carbonyl substrates. We recently discovered that the cationic Ru−H complex $[(C_6H_6)(PCy_3)(CO)\ RuH]^+BF_4^-$ (**1**) with 3,4,5,6-tetrachloro-1,2-benzoquinone (**L1**) is a highly effective catalytic system for mediating the deaminative coupling reaction of ketones with amines to form α-alkylated ketone products.[16] In a subsequent study, we found that the same catalyst system **1**/**L1** selectively promotes the dehydrative coupling reaction of enones with indoles, in which a regioselective C−C bond cleavage of the carbonyl substrates has been achieved in forming 3-alkylindole products.[17] We hypothesized that a regioselective catalytic C−C activation method for carbonyl compounds might be attainable by merging the deaminative coupling protocol with ligand-enabled hydrogen borrowing technology (Scheme 1E).[18] Herein, we report the substrate scope and synthetic utility of a highly regioselective C_α−C_β cleavage method for enones, which is enabled by the ruthenium-catalyzed deaminative coupling reaction with simple amines and anilines. We also delineate combined experimental and computational studies for probing a detailed mechanism of the catalytic coupling reaction as well as for uncovering deep insights on the C−C bond cleavage process.

RESULTS AND DISCUSSION

Reaction Development and Optimization. At the onset of our investigation, we have been searching for a number of different nitrogen-containing substrates that could serve as a removable directing group for promoting the C−C cleavage reactions carbonyl compounds. We initially discovered that the coupling reaction of 1-octen-3-one with 4-methoxybenzylamine led to a regioselective C_α−C_β cleavage of the enone substrate in forming the deaminative coupling product **2a** (eq 1). The formation of both $CH_3NHCH_2C_6H_4$-4-OMe and ammonia byproducts was also detected in the crude mixture. The subsequent optimization and screening efforts established the cationic Ru−H complex **1** with 3,4,5,6-tetrachloro-1,2-benzoquinone (**L1**) as the most effective catalytic system

Table 1. Selected Catalyst Screening and Optimization Study for the Coupling of 1-Octen-3-one with 4-Methoxybenzylamine

entry	catalyst	deviation from standard conditions[a]	**2a** (%)[b]
1	**1**	none	78
2	**1**	with H_2 (5 atm)	75
3	**1**	without **L1**	18
4	**1**	with 2,3-dihydroxynaphthalene (10 mol %)	66
5	$(PCy_3)_2(CO)Ru(O-O)$[c]	without **L1**	66
6	$[(PCy_3)_2(CO)(CH_3CN)_2RuH]^+BF_4^-$		19
7	$[(PCy_3)(CO)RuH]_4(O)(OH)_2/HBF_4{\cdot}OEt_2$		64
8	$(PCy_3)_2(CO)RuHCl/HBF_4{\cdot}OEt_2$		25
9	$RuCl_2(PPh_3)_3/HBF_4{\cdot}OEt_2$		0
10	$Ru_3(CO)_{12}/HBF_4{\cdot}OEt_2$		5
11	$[(COD)RuCl_2]_x/HBF_4{\cdot}OEt_2$		0
12	$PCy_3/HBF_4{\cdot}OEt_2$		0
13	$AlCl_3$		0
14	$HBF_4{\cdot}OEt_2$		0

[a]Standard conditions: 1-octen-3-one (0.5 mmol), 4-methoxybenzylamine (1.0 mmol), catalyst (5 mol %), **L1** (10 mol %), 2-propanol (1.0 mmol), 1,4-dioxane (1 mL), 135 °C, 20 h. [b]The product yield was determined by GC-MS by using hexamethylbenzene as an internal standard. [c]O−O = 3,5-di-*tert*-butylbenzene-1,2-*bis*(olate).

https://doi.org/10.1021/acs.organomet.3c00321
Organometallics 2023, 42, 2867−2880

Table 2. Deaminative Coupling Reaction of Enones with Amines via C−C Cleavage[a]

entry	enone	amine	product	yield (%)
1 2 3	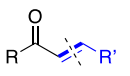	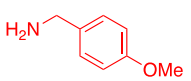	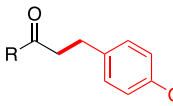	**2a** R = *n*-pentyl R' = H 76 **2b** R = *n*-Bu R' = Me 80 **2c** R = *s*-Bu R' = Me 74
4 5 6 7	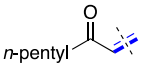	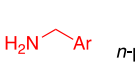	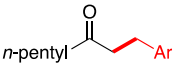	**2d** Ar = Ph 64 **2e** Ar = C_6H_4-4-Me 80 **2f** Ar = C_6H_4-4-Cl 60 **2g** Ar = C_6H_4-4-F 50
8 9	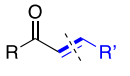	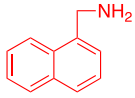	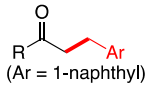	**2h** R = *n*-pentyl R' = H 77 **2i** R = Et R' = Me 74
10 11 12	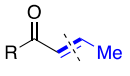	n = 1 n = 3 n = 4 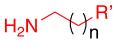	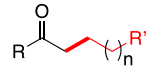	**2j** R = *n*-pentyl R' = Ph 70 **2k** R = *n*-Bu R' = Ph 75 **2l** R = *s*-Bu R' = Me 72
13 14	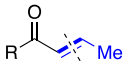	n = 1 n = 2 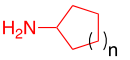	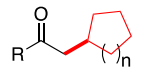	**2m** R = Ph 71 **2n** R = *n*-Bu 68
15	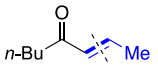	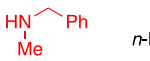	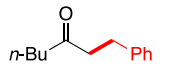	**2o** 43
16 17	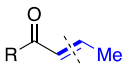	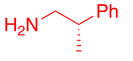	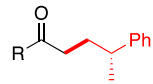	(+)-**2p** R = Et 63 (+)-**2q** R = *s*-Bu 70
18	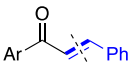		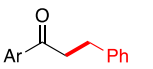	**2r** Ar = C_6H_4-4-OMe 53
19	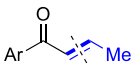	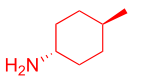	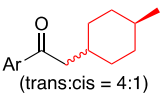	**2s** Ar = C_6H_4-4-OMe 58
20	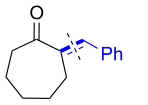	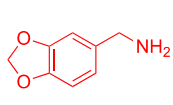	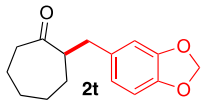	65
21	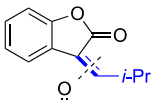	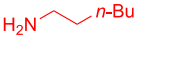	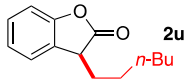	**2u** 69
22	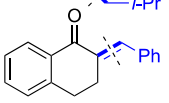	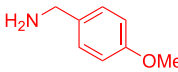	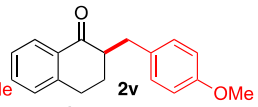	59
23	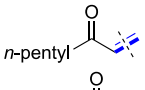	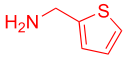	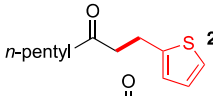	**2w** 63
24	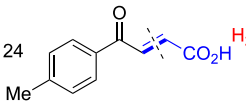			68

[a]Reaction conditions: enone (0.5 mmol), amine (1.0 mmol), **1** (5 mol %), **L1** (10 mol %), 2-propanol (1.0 mmol), 1,4-dioxane (1.5 mL), 135 °C, 20 h.

among screened ruthenium catalysts and catechol and benzoquinone ligands in forming the C−C cleavage product **2a** (Table S1, Supporting Information). Both the in situ formed Ru complex with an electron-deficient 1,2-catechol ligand and a presynthesized Ru-catecholate complex were found to exhibit a high catalytic activity (Table 1, entries 4,5).[16a] Although both H_2 (5 atm) and 2-propanol were found to be equally effective as the hydrogen donor for the coupling reaction (entries 1,2), we employed 2-propanol as the hydrogen source in most catalytic reactions for the sake of convenience, where 1,4-dioxane was found to be the most suitable solvent among common organic solvents. The catalytic method achieves a highly regioselective C_α−C_β bond cleavage of an unstrained enone substrate, in which the hydrogen borrowing protocol has been merged with the deaminative coupling reaction of a simple amine in forming the coupling product **2a**.

Reaction Scope. We surveyed the scope of both enone and amine substrates to probe the C−C cleavage pattern of the coupling reaction under the standard conditions established in Table 1 (Table 2). The coupling reaction of terminal and

https://doi.org/10.1021/acs.organomet.3c00321
Organometallics 2023, 42, 2867−2880

internal enones with benzylic amines cleanly formed ketone products **2a−g** (entries 1−7). The coupling reaction of internal enones with both benzylic and aliphatic amines also led to the ketone products **2h−l**, which resulted from the regioselective $C_\alpha-C_\beta$ cleavage of the enones (entries 8−12). The coupling reaction of enones with primary amines bearing a cyclic group as well as a secondary benzylic amine predictively formed the ketone products **2m−o** (entries 13−15). The reaction with a chiral amine (*R*)-(+)-*β*-methylphenethylamine afforded the coupling products (+)-**2p,q** without any measurable racemization (entries 16 and 17). In contrast, the coupling reaction with *trans*-4-methylcyclohexylamine led to a mixture of the product **2s** (trans/cis = 4:1) resulting from a significant cis/trans isomerization on the amino carbon (entry 19). The coupling of cyclic enones bearing an *exo*-alkenyl group with both benzylic and aliphatic amines smoothly yielded *α*-alkylated ketone products **2t−v** (entries 20−22). The couplings of heteroatom functionalized substrates, 1-octen-3-one with 2-thiophenemethanamine and 3-(4-methylbenzoyl) acrylic acid with 4-methoxybenzylamine, yielded **2w** and **2x**, respectively. Other conjugated carbonyl compounds, such as alkenyl amides and esters as well as *α,β*-unsaturated aldehydes, did not yield any C−C cleavage products under the standard conditions, resulting in a mixture of simple 1,2- and 1,4-addition products. The catalytic method provides a generally applicable $C_\alpha-C_\beta$ cleavage protocol for enone substrates, which has been enabled by merging the hydrogen borrowing technology with the deaminative coupling protocol.

Since the arene C−N bond is considerably stronger than the aliphatic ones, we reasoned that the coupling reaction with aniline substrates might lead to simple C−C cleavage products without the deamination reaction. We next explored the reaction of enones with aniline substrates to examine the C−C bond cleavage pattern in the formation of the coupling products. Indeed, the treatment of a slight excess of 5-methylhept-2-en-4-one (0.75 mmol) with 4-methoxyaniline (0.5 mmol) under otherwise the standard conditions as stipulated in Table 1 led to the formation of a 3:1 mixture of **3a** and **4a** in 93% combined yield (eq 2). The branched

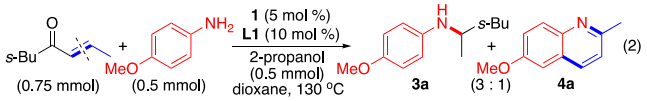

alkyl moiety of the aniline product **3a** clearly indicates a regioselective $C_\alpha-C_\beta$ cleavage of the enone substrate, while the quinoline product **4a** was apparently resulted from combining two equiv of "ethylidene" moieties of the enone substrate.

We surveyed the enone and aniline substrates' scope to probe the C−C cleavage pattern in forming the coupling products (Table 3). The coupling of internal enones with *para*-substituted anilines formed a mixture of the aniline products **3a−d** and quinoline products **4a−d** in excellent combined yields (entries 1−4). In contrast, the coupling of linear enones bearing a terminal olefinic group with anilines formed the aniline products **3e,f** predominantly with <10% of quinoline products in the crude mixture. The coupling of 1-octen-3-one with 1-naphthylamine, 1-anthracenamine, and *para*-substituted anilines formed the corresponding products **3g−i** bearing the branched aliphatic group. On the other hand, the coupling reaction of enones bearing a long-chained *β*-aliphatic group with *para*-substituted anilines predominantly formed 2,4-disubstituted quinoline products **4k,l**, in which two equiv of the *β*-alkyl moieties have been selectively incorporated (entries 11 and 12). The coupling reaction of cyclic enones with the *exo*-alkenyl group with anilines also formed the 2,4-disubstituted quinoline products **4m−4o** (entries 13−16). The formation of these 2,4-disubstituted quinoline products **4** can be readily rationalized from the self-condensation and deaminative annulation reactions of initially formed **3**.

We performed the deaminative coupling reaction by using a number of biologically active enone and amine substrates to demonstrate the synthetic utility of the catalytic C−C cleavage method (Table 4). For example, the treatment of 1-octen-3-one with (−)-*cis*-myrtanylamine and (+)-dehydroabietylamine led to diastereoselective formation of coupling products **2y** and **2z**, respectively. In contrast, the coupling reaction of 1-phenyl-2-buten-1-one with geranylamine formed coupling product **2aa** with a partially hydrogenated proximal olefinic group. The coupling reaction of 1-octen-3-one with heteroatom-containing amino substrates such as (*L*)-tryptophan and 4-morpholinobenzylamine smoothly afforded products **2bb** and **2cc**, respectively. The coupling of a steroid derivative (*E*)-16-benzyliden-3b-hydroxyestra-1,3,5(10)-trien-17-one with *n*-hexylamine formed a diastereomeric mixture of the *α*-alkylated ketone product **2dd**, while the analogous treatment of (*E*)-21-benzyliden-3-hydroxypregn-5-en-20-one with 1-amino-3-methylbutane predictively yielded the corresponding deaminative coupling product **2ee**. We also employed a number of biomass-derived enone substrates for the deaminative coupling reaction with simple amine and aniline substrates. Thus, the treatment of icos-1-en-3-one with 4-methoxybenzylamine under the standard conditions formed the ketone product **2ff** and resulted from the regioselective $C_\alpha-C_\beta$ cleavage of the enone substrate. The analogous treatment of an internal enone bearing a long aliphatic chain heptacos-12-en-14-one with benzo[*d*][1,3]dioxol-5-amine led to a 1:2 mixture of aniline and quinoline products **3p** and **4p** in a 33% combined yield. These examples illustrate synthetic applicability of the C−C cleavage method from harnessing biomass-derived enone and amine substrates.

Reaction Profile and Deuterium Labeling Study. In an effort to establish the reaction sequence, we monitored the coupling reaction of an enone with an amine by using the NMR spectroscopic method. We employed an enone substrate having two different aryl groups in order to distinguish the structure of the intermediate species. Thus, the treatment of 3-(4-chlorophenyl)-1-(4-methoxyphenyl)prop-2-en-1-one (0.25 mmol) with benzylamine (0.25 mmol) in the presence of the complex **1** (5 mol %), **L1** (10 mol %), and 2-propanol (0.50 mmol) in toluene-d_8 (0.5 mL) in a resealable NMR tube was immersed an oil bath set at 135 °C. The tube was periodically taken out of the oil bath, and the ^{1}H NMR spectrum was recorded at an ambient temperature (Figure 1). Initially, rapid formation of the *β*-aminoimine product **5a** was observed, which reached its maximum concentration at 40 min of the reaction time. The formation of the C−C cleaved imine product **6a** was observed at the expense of **5a**, and its maximum concentration was reached at approximately 80 min of the reaction time. The imine **6a** was found to be gradually converted to final ketone product **2r** within 2 h under the stipulated reaction conditions. The results clearly indicated that the coupling reaction proceeds in a consecutive fashion via first the formation of *β*-aminoimine **5a**, which is formed from the initial dehydrative coupling and conjugate addition of amines, followed by the formation of imine **6a**, which results

https://doi.org/10.1021/acs.organomet.3c00321
Organometallics 2023, 42, 2867−2880

Table 3. Coupling Reaction of Enones with Anilines via $C_\alpha-C_\beta$ Cleavage[a]

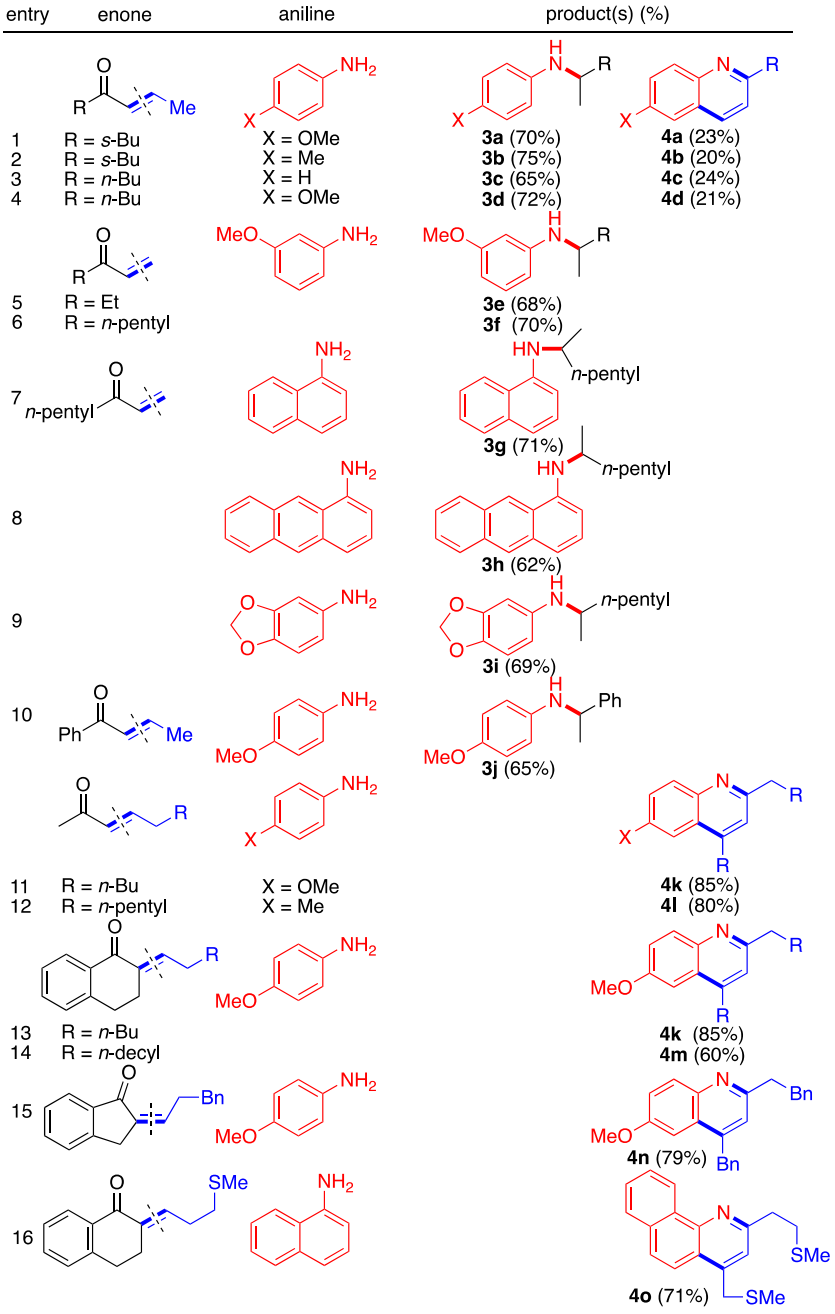

[a]Reaction conditions: enone (0.75 mmol), aniline (0.5 mmol), **1** (5 mol %), **L1** (10 mol %), 2-propanol (0.5 mmol), 1,4-dioxane (1.5 mL), 130 °C, 20 h.

from the C−C bond hydrogenolysis of **5a**, and the eventual formation of the ketone product **2r**.

In a separate experiment, the kinetics on the formation of **2r** was measured by using an independently synthesized imine substrate *N*-(1-(4-methoxyphenyl) ethylidene)-1-phenylmethanamine (**6a**) under the standard conditions (Figure S8, Supporting Information). The plot of initial rate as a function of [**6a**] at four different concentrations (0.4, 0.6, 0.8, and 1.0 mM) showed the first-order dependence on the imine substrate, which translates into the rate constant of $k = 2.6 \times 10^{-3}$ s^{-1}. The kinetics of catalyst dependence was similarly measured at four different concentrations of **1** (0.06−0.012 mM), which also showed the first-order dependence on the Ru catalyst. Since water is needed for the conversion to the ketone product when imine was used as the substrate, we also checked its rate dependence under otherwise standard conditions. The reaction rate was found to be independent of water concentrations in the catalytically relevant range of $[H_2O]$ = 6−1.2 mM. The first-order dependence on [**6a**] suggests that C−N cleavage is the turnover-limiting step of the coupling reaction.

To examine the H/D exchange pattern, we performed the coupling reaction of 2-octen-4-one (0.50 mmol) with α,α-benzylamine-d_2 (0.70 mmol, 98% D) in the presence of complex **1** (5 mol %)/**L1** (10 mol %) and 2-propanol-d_8 (99.5% D, 0.5 mmol) in 1,4-dioxane (1.5 mL) at 135 °C (eq

https://doi.org/10.1021/acs.organomet.3c00321
Organometallics 2023, 42, 2867−2880

Table 4. Coupling Reaction of Biologically Active Enones with Amines and Anilines via C_α–C_β Cleavage[a]

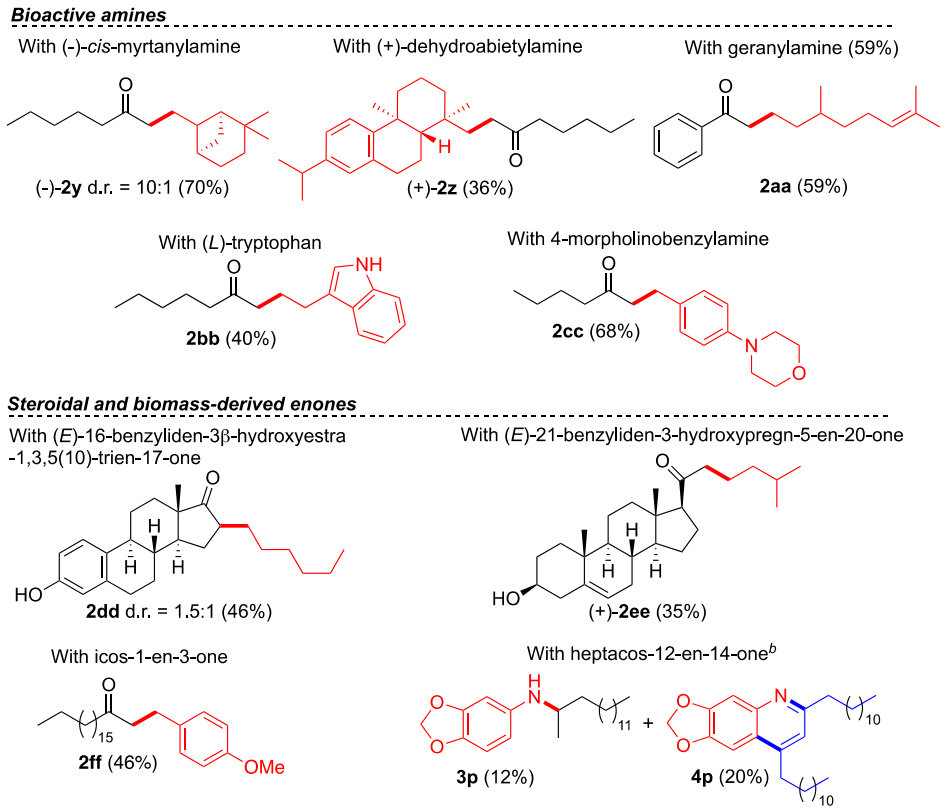

[a]Reaction conditions: enone (0.5 mmol), amine (1.0 mmol), **1** (5 mol %), **L1** (10 mol %), 2-propanol (0.5 mmol), 1,4-dioxane (1.5 mL), 130 °C, 20 h. [b]Enone (0.75 mmol) and aniline (0.5 mmol) were used.

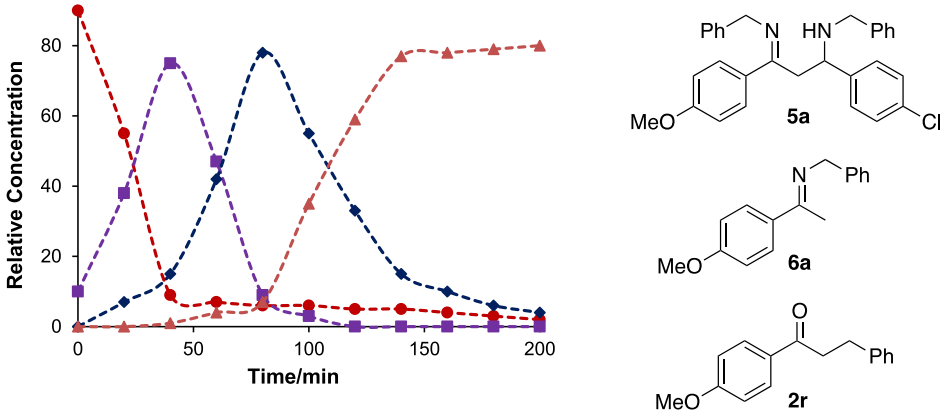

Figure 1. Reaction profile for the coupling of 3-(4-chlorophenyl)-1-(4-methoxyphenyl)prop-2-en-1-one with benzylamine. 3-(4-Chlorophenyl)-1-(4-methoxyphenyl)prop-2-en-1-one (red ●), **5a** (purple ■), **6a** (blue ♦), and **2r** (orange ▲).

3). The isolated product **2o–d** showed that only 55% of deuterium still remains on the benzyl carbon, as a significant

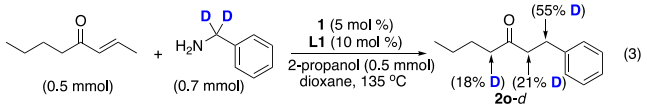

amount of deuterium has been incorporated into both α-CH_2 alkyl groups (18–21% D) as analyzed by ^1H and ^2H NMR spectroscopy (Figure S2, Supporting Information). In a control experiment, the heating of isolated product **2o** (0.25 mmol) with 2-propanol-d_8 (0.25 mmol) under otherwise standard conditions led to nearly identical amounts of deuterium on both α-CH_2 groups without a significant deuterium incorporation on the benzylic carbon (Figure S3, Supporting Information). The observation that nearly half of the deuterium from the benzylamine substrate was spilled over to the α-carbon of the coupling product **2o** suggests a reversible H/D exchange process possibly via an imine-enamine tautomerization and the reversible exchange with 2-propanol.

Hammett Correlation and Carbon Kinetic Isotope Effect Study. We initially hypothesized that either C–C or C–N cleavage would be the most energetically demanding step of the coupling reaction. To probe the electronic influence of the amine substrates on the C–N cleavage process, we

https://doi.org/10.1021/acs.organomet.3c00321
Organometallics 2023, 42, 2867–2880

compared the rate of the coupling reaction of (*E*)-2-octen-4-one with a series of *para*-substituted benzylamines *p*-X-$C_6H_4CH_2NH_2$ (X = OMe, Me, H, F, Cl, and CF_3) under the standard conditions (eq 4). The k_{obs} for each reaction was

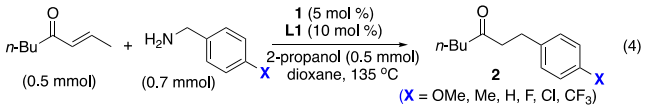

(4)

determined from a first-order plot of $-\ln[((E)\text{-2-octen-4-one})_t/((E)\text{-2-octen-4-one})_0]$ versus time. The Hammett plot of $\log(k_X/k_H)$ versus σ_p showed a linear correlation, in which the coupling reaction is promoted by benzylamines with an electron-releasing group ($\rho = -0.77 \pm 0.1$) (Figure 2). The

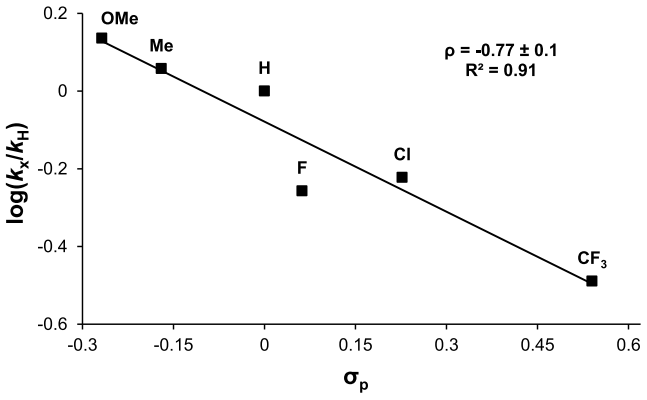

Figure 2. Hammett plot from the coupling reaction of 2-octen-4-one with *p*-X-$C_6H_4CH_2NH_2$ (X = OMe, Me, H, F, Cl, and CF_3).

Hammett data clearly indicate the C−N cleavage (not the C−C cleavage) as the most likely slow step for the coupling reaction. We previously observed a similar Hammett trend in the deaminative alkylation reaction of ketones with amines, where the C−N cleavage was found to be the turnover-limiting step.[16a]

To further discern between C−C versus C−N cleavage turnover-limiting step of the coupling reaction, we measured the carbon kinetic isotope effect (KIE) from the coupling reaction of (*E*)-2-octen-4-one with 4-methoxybenzylamine by employing Singleton's high-precision NMR technique at natural abundance (eq 5).[19] A high conversion sample of **2b**

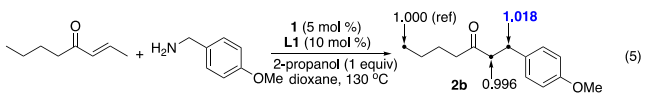

(5)

was obtained from three separate treatments of (*E*)-2-octen-4-one (0.50 mmol) with 4-methoxybenzylamine (1.0 mmol) under the standard reaction conditions (average 82% conversion). A low conversion sample of **2b** was similarly isolated from six separate reactions of (*E*)-2-octen-4-one (1.5 mmol) with 4-methoxybenzylamine (3.0 mmol) under the standard reaction conditions after 2 h of the reaction time (average 13% conversion). The most significant carbon KIE was observed on the benzylic carbon of the product **2b** when the ^{13}C ratio of the product sample obtained from a high conversion was compared with the sample obtained from a low conversion [^{13}C(avg 82% conversion)/^{13}C(avg 13% conversion) at C(1) = 1.018; average of two runs; Table S2, Supporting Information]. The observation of significant carbon KIE on the benzylic carbon further corroborates with the Hammett data that the C−N bond cleavage is the most likely turnover-limiting step of the coupling reaction.

DFT Computational Study. We performed density functional theory (DFT) calculations to attain deeper mechanistic insights into the coupling reaction. We previously established an unsaturated Ru-catecholate complex as the catalytically active species for the deaminantive coupling reaction of ketones with amines.[16a] By using the same Ru-catecholate framework, we initially explored a number of plausible reaction sequences to identify a low energy pathway for the entire catalytic cycle. Since the experimental reaction profile study identified an *β*-aminoimine **5** as the initially formed substrate, we employed the optimized structure of Ru-catecholate-imine complex **A1** as the starting point to probe various reaction pathways for the coupling reaction. The calculations were performed at the PBE/ma-def2-TZVPP level of theory with SMD solvent model and D4 model for the dispersion interactions, and the computational details are summarized in Supporting Information.[20] To reduce the computational time, we optimized the Ru complexes bearing PMe_3 instead of PCy_3 and the catecholate ligand without Cl atoms.

We first identified that the Ru-aminoimine complex **A1** proceeds with a highly endergonic rearrangement step, which essentially replaces the Ru-amine dative bond with an agostic interaction between the Ru atom and the *γ*-C−H bond in forming **A2** (Figure 3). The reaction step was found to have a high energy barrier ($\Delta G^{\ddagger}$ = 31.1 kcal/mol) with ΔG = 22.2 kcal/mol from **A1** to **A2**. The Ru−N bond distance was found to be considerably elongated (2.62 Å) in transition state **TS1**, while a significant Ru *γ*-C−H agostic bonding interaction is established, as indicated by a relatively short Ru−H bond distance of 2.30 Å. The geometrical parameters as indicated by relatively short bond distances, Ru−N (3.15 Å), Ru−H (1.80 Å), and Ru−C (2.55 Å), also suggest of a relatively strong agostic interaction in **A2**. The agostic complex **A2** readily inserts the *γ*-C−H bond to form five-membered metallacyclic Ru−H species **A3**. The insertion process has a relatively low energy barrier ($\Delta G^{\ddagger}$ = 7.3 kcal/mol), with an overall uphill process from **A2** (ΔG = 7.8 kcal/mol) and corresponding electronic energies ($\Delta E^{\ddagger}$ = 8.4 and ΔE = 8.1 kcal/mol). In the geometrically optimized transition state **TS2**, the *γ*-C−H bond is significantly elongated to 1.53 Å, while both the Ru−H and Ru−C bond distances are decreased to 1.58 and 2.23 Å, respectively. The resulting complex **A3** readily proceeds via a 1,3-proton transfer with a relatively low activation barrier via **TS3** ($\Delta G^{\ddagger}$ = 6.2 kcal/mol), and this step is energetically downhill (ΔG = −16.5 kcal/mol) in forming **A4**. It is noteworthy that the activation barrier is further reduced in the presence of an external acid (e.g., 1.2 kcal/mol lower with NH_4^+), which alleviates the strain energy typically associated with an intramolecular 1,3-proton transfer process. We also investigated **A2**-**A4** transformation by using the nudged elastic band (NEB) method to differentiate between stepwise versus concerted pathway. The calculations showed that the lowest−energy profile is achieved via intermediate structure **A3**, indicating that the two-step transformation via **A2**-**A3**-**A4** is energetically more favorable than the concerted pathway.

We reasoned that intermediate **A4** could expedite the C−C cleavage reaction via the formation of a stable Fischer-type Ru-aminocarbene species bearing an enamine moiety. After extensive exploratory efforts, we have been able to identify

https://doi.org/10.1021/acs.organomet.3c00321
Organometallics 2023, 42, 2867−2880

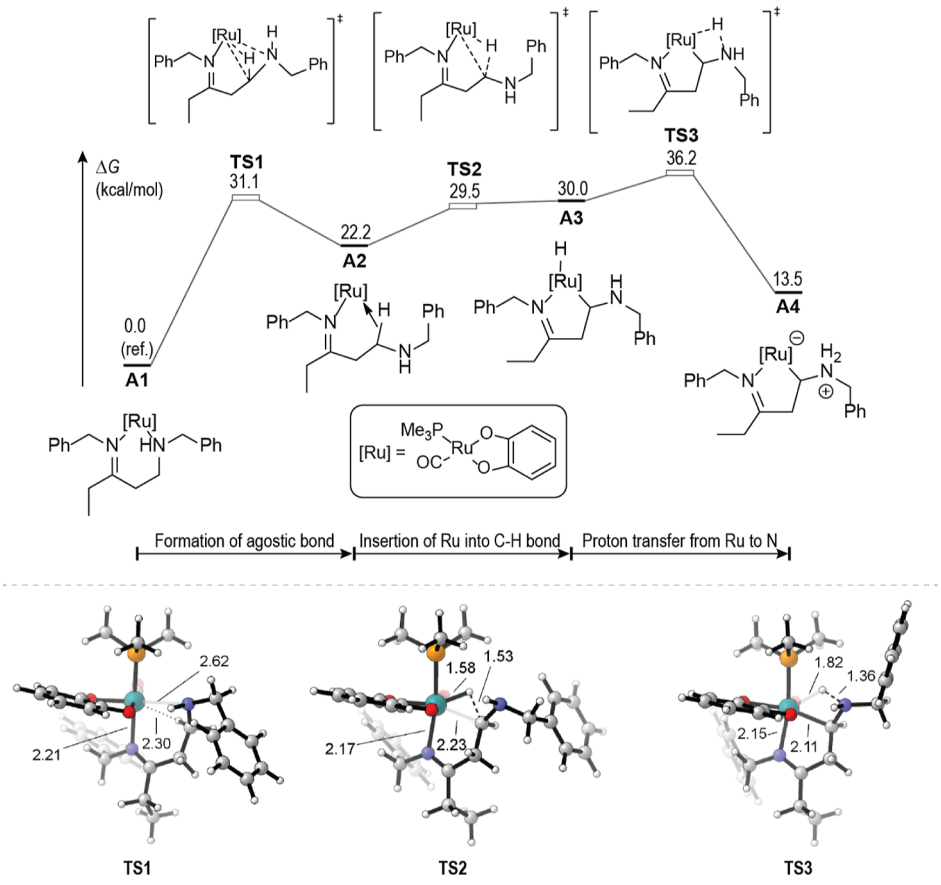

Figure 3. Free energy profile and optimized transition state structures for the transformation of the Ru-aminoimine complex **A1** into the imine complex **A4** [PBE-D4/ma-def2-TZVPP, SMD (1,4-dioxane)].

an energetically feasible C−C cleavage route via the formation of a Ru-aminocarbene species (Figure 4). We computed the energies for the pathway in which **A4** first undergoes a direct proton transfer between the two nitrogen atoms via **TS4** ($\Delta G^{\ddagger}$ = 22.5 kcal/mol, ΔG = 18.5 kcal/mol), which is followed by a conformational reorganization of **A5** via **TS5** ($\Delta G^{\ddagger}$ = 4.2 kcal/mol) to form a pivotal intermediate **A8** (**A5** → **A8**, ΔG = −5.4 kcal/mol) (Path A). We subsequently found an alternate pathway for the transformation of **A4** → **A8**, which involves a stepwise proton transfer to the catechol oxygen atom via **TS4'** ($\Delta G^{\ddagger}$ = 13.1 kcal/mol) with the overall ΔG = 10.8 kcal/mol for **A4** → **A6** (Path B). The calculations showed that the latter path has a considerably lower energy barrier on the first proton transfer step (**TS4** vs **TS4'** $\Delta\Delta G^{\ddagger}$ = 9.4 kcal/mol) as well as on the subsequent proton transfer steps ($\Delta\Delta G^{\ddagger}$ = 2.4 kcal/mol) compared to the former pathway. We considered yet another possible route via a direct proton transfer from Ru to the oxygen atom of catechol ligand **A4** → **A7**, but the calculations showed that this direct proton transfer path has an unreasonably high energy barrier ($\Delta G^{\ddagger}$ = 47.1 kcal/mol), probably due to a strained nature on the transition state. The intermediate **A6** smoothly undergoes a facile conformational transformation to **A7** via **TS6** ($\Delta G^{\ddagger}$ = 8.6 kcal/mol, ΔG = 7.8 kcal/mol), which is followed by the proton transfer from the oxygen to the nitrogen atom via **TS7** ($\Delta G^{\ddagger}$ = 1.7 kcal/mol) with an overall exergonic process **A7** → **A8** (ΔG = −5.5 kcal/mol). We also considered a concerted path for the C−C bond cleavage step, which occurs in a single elementary step from **A6** to **A9** via transition state **TS6'** ($\Delta G^{\ddagger}$ = 18.0 kcal/mol, ΔG = −13.7 kcal/mol) (Path C). We concluded that this concerted pathway is highly unlikely because it has an energy barrier much higher than either path A or B ($\Delta\Delta G^{\ddagger}$ = 6.1 and 8.5 kcal/mol, respectively).

The calculations revealed that intermediate **A8** is highly amenable to the C−C bond cleavage process via transition state **TS8**. We were initially surprised to learn that the formation of **TS8** requires an exceptionally low free energy of activation ($\Delta G^{\ddagger}$ = 4.5 kcal/mol) with the highly exergonic step **A8** → **A9** (ΔG = −16.0 kcal/mol), despite having a relatively short C−C bond length in **A8** (1.54 Å). The optimized structure of **TS8** displays a smooth evolution of geometrical parameters, as indicated by a lengthening of the C−C bond from **A8** to **TS8** (1.54 to 1.99 Å) as well as a shortening of the Ru−C distance from **A8** to **TS8** and **A9** (2.16, 2.05, and 1.95 Å, respectively). At the same time, **TS8** shows a somewhat unexpected elongation of the Ru−N bond distance (2.83 Å) compared to both **A8** and **A9** (2.22 and 2.28 Å) as well as a significant contraction of the adjacent C−N bond distance (1.34 Å *vs* 1.39−1.44 Å), which suggests a significant contribution of the π-C−N bond character in developing enamine fragment on **TS8**.

To decipher the origin of the facile C−C bond cleavage mechanism, we examined the frontier molecular orbitals for **A8** and **TS8** in detail (Figure 5A). We observed an unusual feature on the frontier orbitals of **TS8** that the HOMO orbital of **TS8** is mostly localized on the catechol fragment and Ru atom without any significant expansion to the nitrogen or carbon atoms involved in the C−C bond cleavage, while the LUMO of

https://doi.org/10.1021/acs.organomet.3c00321
Organometallics 2023, 42, 2867−2880

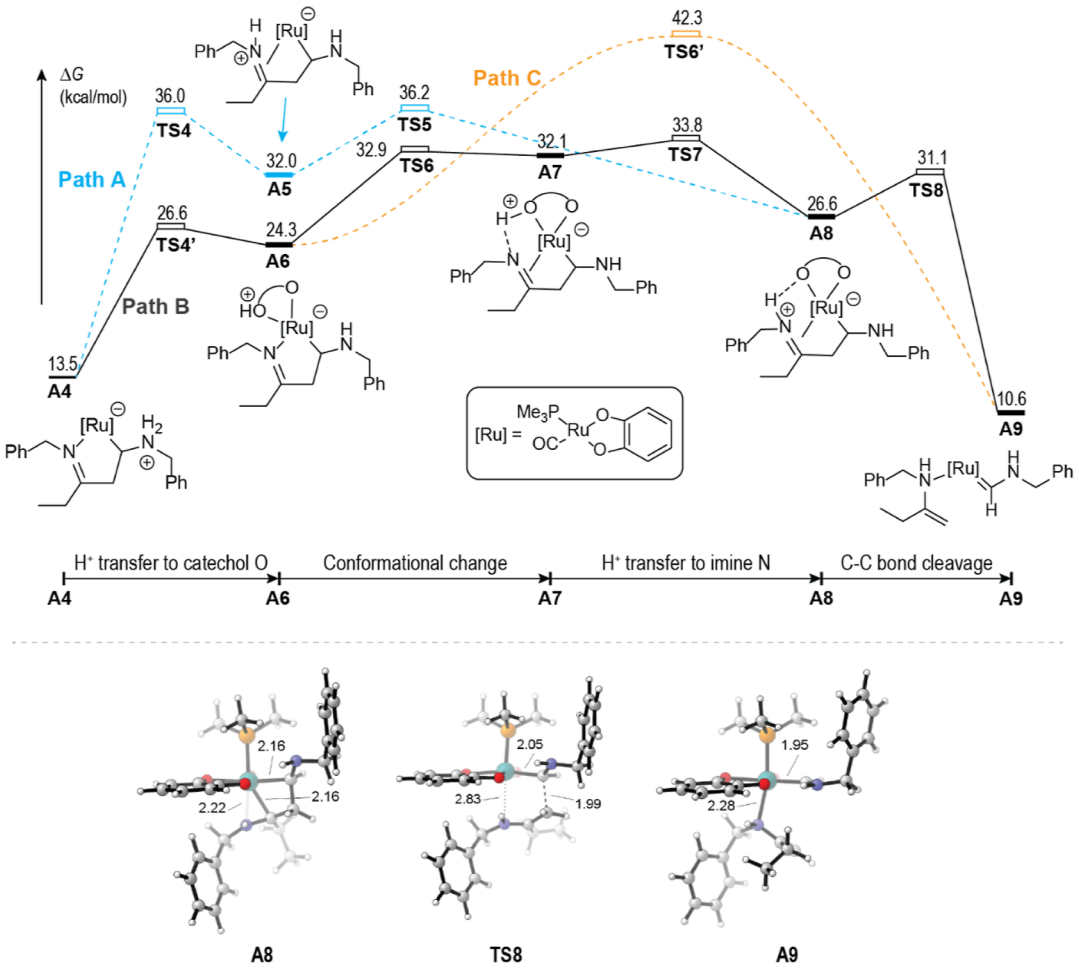

Figure 4. Free energy profiles and selected representative structures for the transformation of the Ru-aminoimine complex **A4** into the imine complex **A9** [PBE-D4/ma-def2-TZVPP, SMD (1,4-dioxane)].

TS8 displays an expected π-type antibonding character on the existing C═N bond. To explain a lack of involvement of HOMO orbitals of **TS8** in the C−C bond cleavage step, we analyzed a corresponding uncatalyzed reaction, where a protonated imine undergoes the C−C bond cleavage reaction to form two double bonds (Figure S7a, Supporting Information). The C−C bond cleavage reaction becomes a highly endergonic process without the Ru catalyst (ΔG = 25.6 kcal/mol), and the NEB calculations on the C−C bond cleavage step displayed a monotonic dissociation curve without an activation barrier or visible shoulder.

We attribute an absence of significant energy barrier to the stability of the intermediate structures along the dissociation curve, resulting from a delocalized 5-orbital 6-electron structure. In fact, a visual inspection of the three highest occupied and two lowest unoccupied molecular orbitals for a representative intermediate structure along the dissociation curve shows that the nodal composition is very similar to the Hückel orbitals of a generic linear 5-orbital 6-electron system (Figure S7b, Supporting Information). The LUMO orbital in this system has a clearly discernible character of two antibonding orbitals for the double bonds in the reactant, whereas the HOMO is composed of three separated p-orbitals with predominantly nonbonding character. Although a similar set of molecular orbitals has been observed in **TS8**, these p-orbitals are not directly involved in the chemical transformation because the structure of **TS8** has a strong contribution from Ru dz-atomic orbital, which has an extensive orbital mixing with p-orbitals from the organic fragments (see Figure S7c, Supporting Information). As a result, we believe that the presence of the Ru moiety facilitates extended delocalization of p-orbitals in the transition states, which lowers the overall dissociation pathway and ultimately results in a low activation barrier for C−C bond cleavage step **A8** → **A9**.

We utilized the intrinsic bond orbital (IBO) method to further analyze the electronic transformation in the C−C bond cleavage step. The IBO method has been well-recognized for its capacity to produce interacting bond orbitals along the reaction profile, which can be easily interpreted by using the electron flow curly arrows.[21] The IBO analysis for the C−C bond cleavage step from **A8** to **A9** yielded three interacting orbitals, and their progression provides a clear interpretation with the three resulting curly arrows, as shown in the structural formula of **A8** in Figure 5B. Taken together, the IBO analysis shows a smooth reorganization of the C−C σ bond into two π-bonds situated on two fragments in **TS8**, which is accompanied by an electron transfer between the two nitrogen atoms.

Fischer-type metal-aminocarbene complexes have been well-known to undergo carbene-to-imine rearrangement to form metal-imine complexes.[22] To illustrate a viable mechanism for

https://doi.org/10.1021/acs.organomet.3c00321
Organometallics 2023, 42, 2867−2880

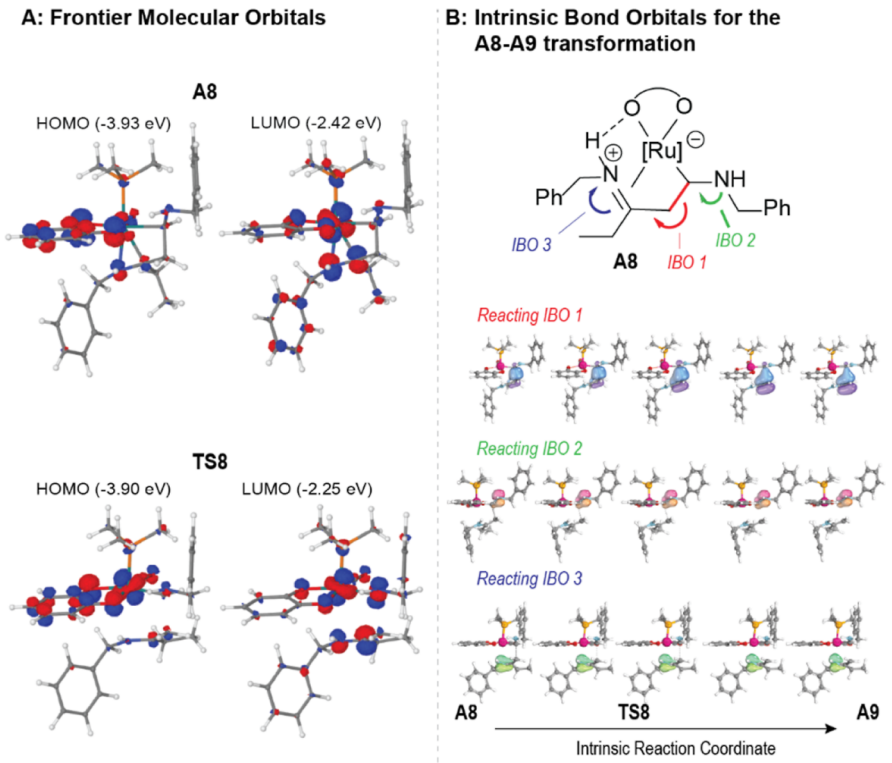

Figure 5. (A) Frontier canonical molecular orbitals for **A8** and **TS8**. (B) Progression of the IBOs representing the C−C bond cleavage along the intrinsic reaction coordinate for transformation **A8** → **A9**. The ball and stick models of **A8** and **TS8** without orbitals are shown in Figure 4.

Scheme 2. Calculated Mechanistic Pathway for the Carbene-to-imine Rearrangement (A9 → A12) and the Formation of Ketone Product 2

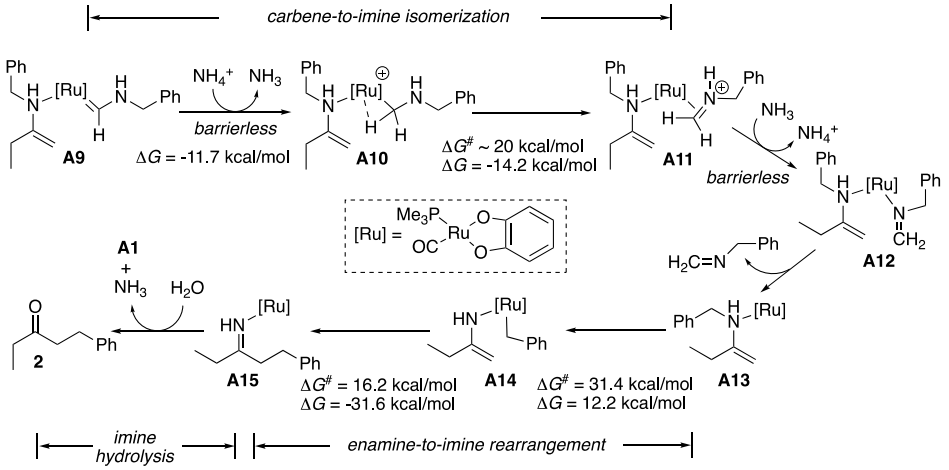

the carbene-to-imine isomerization reaction, we conducted DFT calculations to establish a low energy pathway for the rearrangement of Ru-carbene intermediate **A9** to **A12** (Scheme 2). We found that the carbene carbon of **A9** is readily protonated by an external proton donor such as NH_4^+, leading to Ru-alkyl species **A10** without any measurable activation barrier (ΔG = −11.7 kcal/mol). The intermediate **A10** then undergoes an endergonic rearrangement process, leading to π-C═N bond coordination to the Ru center in forming **A11**. The NEB calculations showed a reasonable pathway with the energy of activation approximately 20.0 kcal/mol; however, we could not obtain an energy-minimized transition state, despite numerous attempts to optimize the possible structures. Finally, the deprotonation (loss of NH_4^+) and the formation of a dative η-type Ru−N bond from **A11** smoothly proceed without any measurable energy barrier to form the imine complex **A12**.

The last phase of the coupling reaction constitutes enamine-to-imine isomerization and imine hydrolysis steps. In the previously reported Ru-catalyzed deaminative alkylation of ketones with amines, we showed that a Ru-catecholate complex effectively mediates the enamine-to-imine rearrangement via a stepwise 1,3-carbon shift mechanism.[16a] The DFT calculations for the enamine-to-imine rearrangement step (**A13** → **A15**) revealed that the enamine-to-imine rearrangement also proceeds in a stepwise fashion with the calculated free energies almost identical to the previously reported ones.

https://doi.org/10.1021/acs.organomet.3c00321
Organometallics 2023, 42, 2867−2880

Moreover, the calculations showed a substantially higher energy barrier for the C−N bond cleavage step ($\Delta G^{\ddagger}$ = 31.4 kcal/mol) (**A13** → **A14**), compared to the C−C bond formation step ($\Delta G^{\ddagger}$ = 16.2 kcal/mol) (**A14** → **A15**). These computational results further validate experimental carbon KIE and Hammett correlation data that the C−N bond cleavage is one of the most energetically demanding steps for the coupling reaction. The final imine hydrolysis from **A15** forms the observed ketone product **2** along with the regeneration of **A1**.

The DFT calculations predicted that the C−H and C−N bond cleavage processes are the two most energetically demanding steps in the coupling reaction. To conform to the energetically demanding nature of the C−H bond activation step, we measured a deuterium KIE from the reaction of 4-methoxybenzylamine with 4-OMeC$_6$H$_4$COCH═CHPh versus 4-OMeC$_6$H$_4$COCH═CDPh under parallel conditions. In two separate NMR tubes, each containing 4-methoxybenzylamine (0.50 mmol), 4-OMeC$_6$H$_4$COCH═CHPh (0.13 mmol), or 4-OMeC$_6$H$_4$COCH═CDPh (0.13 mmol), complex **1** (5 mol %), **L1** (10 mol %), and 2-propanol (0.50 mmol) in toluene-d_8 (0.5 mL) was heated in an oil bath set at 135 °C. To ensure reliable rate measurement for the C−H bond activation step, we began the rate measurement at 30 min for each reaction, at which time the formation of **5a** has reached its maximum concentration, as illustrated in the reaction profile study. Each reaction tube was taken out of the oil bath in 20 min intervals, and the reaction rate was measured by monitoring the appearance of the product signals on ^{1}H NMR. The k_{obs} was determined from a first-order plot of $-ln[(4\text{-OMeC}_6\text{H}_4\text{COCH═CHPh})_t/(4\text{-OMeC}_6\text{H}_4\text{COCH═CHPh})_0]$ versus time and repeated for the deuterated substrate, which clearly showed a normal deuterium KIE value (k_H/k_D = 1.8 ± 0.1) (Figure 6). The experimental results

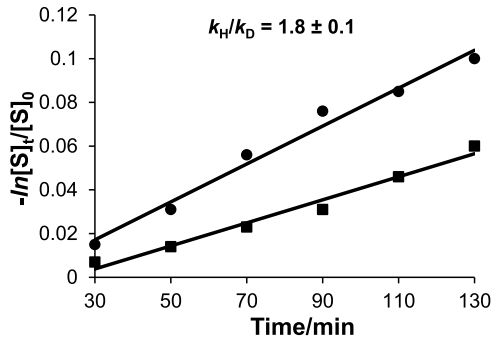

Figure 6. First order plots from the reaction of 4-OMeC$_6$H$_4$COCH═CHPh (●) vs 4-OMeC$_6$H$_4$COCH═CDPh (■) with 4-methoxybenzylamine.

further corroborate the computational prediction that the γ-C−H bond activation is one of the two most energetically demanding steps for the coupling reaction.

Proposed Mechanism. We compiled a plausible mechanistic pathway for the deaminative coupling reaction of an enone with benzylamine on the basis of combined experimental and computational results (Scheme 3). The reaction profile experiment established that the β-aminoimine substrate **5**, which would be initially formed from the dehydrative coupling and conjugate addition reactions of the enone substrate with 2 equiv of benzylamine, is the actual substrate for the Ru catalysis. In light of the previously observed catalytic activity of the Ru-catecholate complex,[16a] we propose that unsaturated Ru-catecholate complex **7**, which is in situ generated from the reductive coupling of Ru−H complex **1** with the benzoquinone ligand **L1**, is the catalytically active species for the reaction. The coordination of β-aminoimine substrate **5** to Ru-catecholate complex **7** would form Ru-catecholate-imine complex **8**, which mediates a highly endergonic γ-C−H insertion reaction to form five-membered ruthenacyclic species **9**. The DFT calculations predicted the C−H insertion step as one of the two most energetically demanding steps for the catalytic coupling reaction ($\Delta G^{\ddagger}$ = 30 kcal/mol). Such an energetically demanding nature of the C−H insertion step has been validated experimentally by the observation of a normal deuterium KIE from the coupling reaction of an enone with benzylamine (k_H/k_D = 1.8 ± 0.1). The DFT calculations also revealed that the Ru−H species **9** proceeds with a series of proton transfer steps in which the catecholate ligand of **9** facilitates a low energy pathway in forming the zwitterionic Ru-iminyl species **10**.

The resulting Ru-iminyl complex **10** is set to undergo the key C−C cleavage reaction to form Ru-carbene species **11**. The DFT calculations established that the Ru-mediated γ-C−H activation and the subsequent proton transfer steps lead to a substantially increased electrophilic character on the iminium nitrogen, which translates into a facile C−C cleavage step with an unusually low energy barrier. The IBO analysis further provided deep mechanistic insight for such facile C−C cleavage step that is characterized by having a smooth orbital transformation of the C−C σ-bond into two different π-bond fragments via the **TS8**. The DFT calculations further revealed a mechanistic rationale where the redox-active catecholate ligand serves as an effective facilitator for channeling a multistep proton transfer process.

The resulting aminocarbene complex **11** rapidly undergoes a carbene-to-imine isomerization reaction to form the Ru-enamine-imine species **12**. The resulting imine moiety would undergo hydrogenation in a separate catalytic process to form the secondary amine byproduct, while the remaining *N*-alkylimine group of **12** proceeds with the 1,3-carbon shift to form the Ru-imine complex **13**. The DFT calculations established that the enamine-to-imine rearrangement (C−N bond cleavage step) occurs in a stepwise fashion via the formation of Ru(IV)-alkyl species in forming Ru-imine complex **13**. The DFT calculations also predicted that the enamine-to-imine rearrangement is one of the two most energetically demanding steps of the coupling reaction ($\Delta G^{\ddagger}$ = 31.4 kcal/mol). The observation of both pronounced carbon KIE on the benzyl carbon as well as the Hammett data provided complementary experimental support for such energetically demanding nature on the C−N cleavage step. Since both C−H cleavage and the 1,3-alkyl migration (C−N cleavage) steps have nearly identical activation energies ($\Delta G^{\ddagger}$ = 31.1 kcal/mol for the C−H cleavage step vs $\Delta G^{\ddagger}$ = 31.4 kcal/mol for the C−N cleavage step), it is likely that the coupling reaction has two separate energetically demanding and rate-determining steps. Finally, the resulting imine from **13** would be rapidly hydrolyzed to form the observed ketone product **2** with the regeneration of the starting Ru-catecholate catalyst **7**.

Overall, the catalytic deaminative coupling method consists of three consecutive reaction stages. The first stage involves the formation of β-aminoimine substrate **5** from the dehydrative coupling and conjugate addition of an enone with a simple amine. In the main catalytic cycle, the Ru-mediated γ-C−H

https://doi.org/10.1021/acs.organomet.3c00321
Organometallics 2023, 42, 2867−2880

Scheme 3. Proposed Mechanistic Pathway for the Deaminative Coupling Reaction of an Enone with Benzylamine via C−C Bond Cleavage

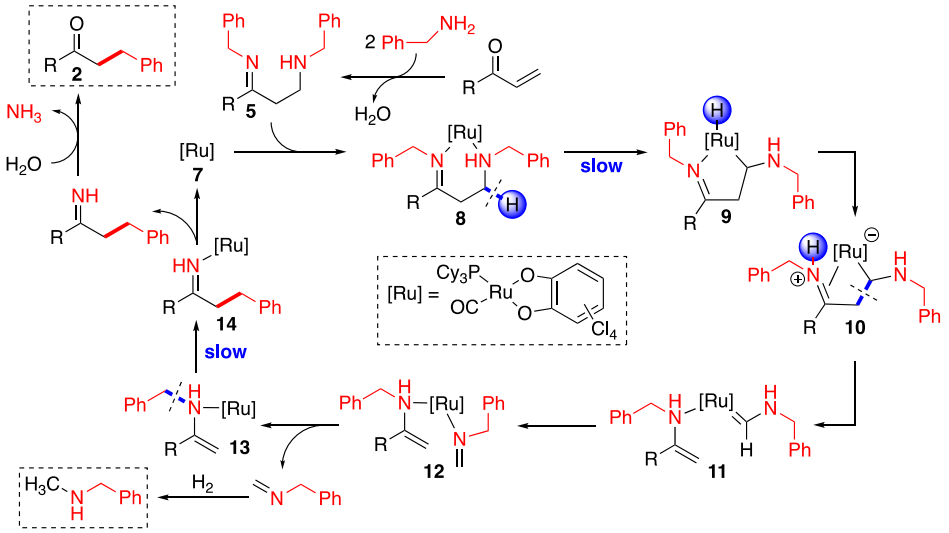

activation and subsequent proton transfer steps facilitate a facile C−C cleavage reaction in forming both enamine and aminocarbene fragments. The resulting aminocarbene fragment readily proceeds with the carbene-to-imine isomerization and separate hydrogenation reactions to form the secondary amine byproduct. Meanwhile, the *N*-alkylenamine group undergoes a highly energetically demanding enamine-to-imine rearrangement, which is followed by the imine hydrolysis reaction to form the observed ketone product **2**.

CONCLUSIONS

In summary, we have successfully developed a generally applicable catalytic C−C bond cleavage method of unstrained enones from the deaminative coupling reaction with amines in forming the elaborated ketone products **2**. The analogous catalytic coupling reaction of enones with anilines produced a mixture of *N*-alkylaniline and 2,4-disubstituted quinoline products **3** and **4**, both of which result from the regioselective C_α−C_β bond cleavage of the enone substrates. The combined experimental and computational studies uncovered a detailed mechanistic picture for the coupling reaction in which an unsaturated Ru-catecholate catalyst facilitates γ-C−H insertion of the initially formed β-aminoimine substrate and the subsequent proton transfer steps to achieve the regioselective C_α−C_β cleavage reaction of enones. The overall mechanistic scheme of the coupling reaction is composed of three consecutive stages: (1) formation of β-aminoimine substrate from the dehydrative coupling and conjugate addition of enone with two equiv of amine substrate, (2) Ru-catalyzed fragmentation of β-aminoimine substrate (C−C cleavage process) and the subsequent enamine-to-imine rearrangement of *N*-alkylenamine (C−N cleavage process), and (3) hydrolysis and hydrogenation reactions of the resulting imines to form the ketone product **2** and the secondary amine byproduct. In short, we have successfully developed a new catalytic C_α−C_β bond cleavage method for unstrained enones by combining hydrogen borrowing and deaminative coupling strategies to form synthetically valuable ketone and quinoline products. We are currently devoting our efforts to further extend substrate scope as well as for exploring synthetic applicability of the catalytic C−C cleavage method in the synthesis of target molecules.

EXPERIMENTAL SECTION

General Procedure for the Coupling Reaction of an Enone with an Amine. In a glovebox, complex **1** (15 mg, 5 mol %), benzoquinone **L1** (12 mg, 10 mol %), and 2-propanol (30 mg, 1 equiv) were dissolved in anhydrous 1,4-dioxane (1.0 mL) in a 25 mL Schlenk tube equipped with a Teflon screw cap stopcock and a magnetic stirring bar. Both enone (0.50 mmol) and amine (1.0 mmol) substrates in 1,4-dioxane (0.5 mL) solution were added to the tube. After the tube was sealed, it was brought out of the glovebox and was stirred in an oil bath set at 135 °C for 20 h. The reaction tube was taken out of the oil bath and allowed to cool to room temperature. After the tube was open to air, the crude mixture was filtered through a short silica gel column by eluting with CH_2Cl_2 (10 mL) and the filtrate was analyzed by GC-MS. Analytically pure product **2** was isolated by simple column chromatography on silica gel (40−63 μm particle size, hexanes/EtOAc) and was fully characterized by spectroscopic methods.

Computational Method. Input models were constructed using Avogadro software[23] and optimized using DFT with the Orca software, version 5.0.3.[24] Geometry optimization calculations were carried out with the PBE[25] functional combined with the D4[26] dispersion correction for a more accurate treatment of the dispersion interactions. Initially, the reaction mechanism was explored using a smaller basis set, def2-SV(P), for computational efficiency.[27] Subsequently, the obtained geometries were reoptimized using a triple-ζ quality basis set, ma-def2-TZVPP.[28] The optimized structures obtained from different basis sets were quite similar to RMSD values typically within 0.1 Å. The relative electronic energies for the entire reaction mechanism, obtained with the double-ζ versus triple-ζ basis set, showed an excellent linear correlation with slope of 1.0061 and intercept of 0.47 kcal/mol (R^2 = 0.995). The electronic flow in the reaction **A8** → **A9** was represented by using the IBO approach as implemented in IboView software.[21,29]

Wave function stability calculations were performed to verify the absence of lower-energy numerical solutions. Additionally, single-point calculations for a triplet electronic state were carried out to confirm that the singlet state was the ground electronic state. Harmonic frequency calculations were performed to determine the nature of the optimized structures. Specifically, all positive frequency values signified that the structure represented a minimum on the potential energy surface, while a single negative frequency value indicated a transition state. The Gibbs free energies were calculated

https://doi.org/10.1021/acs.organomet.3c00321
Organometallics 2023, 42, 2867−2880

based on the obtained geometries and frequencies at T = 298.15 K and P = 1 atm. We used the geometries obtained from the optimization with the triple-ζ basis set in a vacuum as input for a single-point calculation using the SMD solvation model.[30] The parameters for the solvation model were set for the solvent 1,4-dioxane, and all geometries were reoptimized using a polarized continuum solvent model (PCM) for the solvent THF. The free energy profiles obtained from gas-phase, PCM and SMD calculations were found to be very similar, as the inclusion of the PCM model into calculations had only a minor influence on the optimized geometries.

■ ASSOCIATED CONTENT

Supporting Information

The Supporting Information is available free of charge at https://pubs.acs.org/doi/10.1021/acs.organomet.3c00321.

Experimental procedures, characterization data, NMR spectra for organic products, separate computational details, and calculated structures and their Cartesian coordinates (PDF)

DFT structures (XYZ)

■ AUTHOR INFORMATION

Corresponding Authors

Marat R. Talipov − *Department of Chemistry and Biochemistry, New Mexico State University, Las Cruces, New Mexico 88003, United States;* orcid.org/0000-0002-7559-9666; Email: talipovm@nmsu.edu

Chae S. Yi − *Department of Chemistry, Marquette University, Milwaukee, Wisconsin 53233, United States;* orcid.org/0000-0002-4504-1151; Email: chae.yi@marquette.edu

Author

Dulanjali S. Thennakoon − *Department of Chemistry, Marquette University, Milwaukee, Wisconsin 53233, United States*

Complete contact information is available at: https://pubs.acs.org/10.1021/acs.organomet.3c00321

Notes

The authors declare no competing financial interest.

■ ACKNOWLEDGMENTS

Financial support from the National Science Foundation (CHE-2153885) is gratefully acknowledged. The DFT calculations were performed using the resources provided by Extreme Science and Engineering Discovery Environment (XSEDE) TG-CHE170004.

■ REFERENCES

(1) Recent reviews: (a) Marek, I.; Masarwa, A.; Delaye, P.-O.; Leibeling, M. Selective Carbon−Carbon Bond Cleavage for the Stereoselective Synthesis of Acyclic Systems. *Angew. Chem., Int. Ed.* **2014**, *54*, 414−429. (b) Souillart, L.; Cramer, N. Catalytic C−C Bond Activations via Oxidative Addition to Transition Metals. *Chem. Rev.* **2015**, *115*, 9410−9464. (c) Nairoukh, Z.; Cormier, M.; Marek, I. Merging C−H and C−C bond cleavage in organic synthesis. *Nat. Rev. Chem.* **2017**, *1*, 1−17. (d) Xia, Y.; Dong, G. Temporary or removable directing groups enable activation of unstrained C−C bonds. *Nat. Rev. Chem.* **2020**, *4*, 600−614.

(2) (a) de Lasa, H.; Salaices, E.; Mazumder, J.; Lucky, R. Catalytic Steam Gasification of Biomass: Catalysts, Thermodynamics and Kinetics. *Chem. Rev.* **2011**, *111*, 5404−5433. (b) Serrano-Ruiz, J. C.; Luque, R.; Sepúlveda-Escribano, A. Transformations of biomass-derived platform molecules: from high added-value chemicals to fuels via aqueous-phase processing. *Chem. Soc. Rev.* **2011**, *40*, 5266−5281. (c) Zhang, C.; Shen, X.; Jin, Y.; Cheng, J.; Cai, C.; Wang, F. Catalytic Strategies and Mechanism Analysis Orbiting the Center of Critical Intermediates in Lignin Depolymerization. *Chem. Rev.* **2023**, *123*, 4510−4601.

(3) (a) Cohen, Y.; Cohen, A.; Marek, I. Creating Stereocenters within Acyclic Systems by C−C Bond Cleavage of Cyclopropanes. *Chem. Rev.* **2021**, *121*, 140−161. (b) Fumagalli, G.; Stanton, S.; Bower, J. F. Recent Methodologies That Exploit C−C Single-Bond Cleavage of Strained Ring Systems by Transition Metal Complexes. *Chem. Rev.* **2017**, *117*, 9404−9432.

(4) (a) Gozin, M.; Weisman, A.; Ben-David, Y.; Milstein, D. Activation of a carbon−carbon bond in solution by transition-metal insertion. *Nature* **1993**, *364*, 699−701. (b) Rybtchinski, B.; Vigalok, A.; Ben-David, Y.; Milstein, D. A Room Temperature Direct Metal Insertion into a Nonstrained Carbon-Carbon Bond in Solution. C−C vs C−H Bond Activation. *J. Am. Chem. Soc.* **1996**, *118*, 12406−12415.

(5) (a) Chen, F.; Wang, T.; Jiao, N. Recent Advances in Transition Metal-Catalyzed Functionalization of Unstrained Carbon-Carbon Bonds. *Chem. Rev.* **2014**, *114*, 8613−8661. (b) Song, F.; Gou, T.; Wang, B.-Q.; Shi, Z.-J. Catalytic activations of unstrained C−C bond involving organometallic intermediates. *Chem. Soc. Rev.* **2018**, *47*, 7078−7115.

(6) (a) Park, Y. J.; Park, J.-W.; Jun, C.-H. Metal-Organic Cooperative Catalysis in C−H and C−C Bond Activation and Its Concurrent Recovery. *Acc. Chem. Res.* **2008**, *41*, 222−234. (b) Kim, D.-S.; Park, W.-J.; Jun, C.-H. Metal−Organic Cooperative Catalysis in C−H and C−C Bond Activation. *Chem. Rev.* **2017**, *117*, 8977−9015.

(7) (a) Rodríguez, N.; Goossen, L. J. Decarboxylative coupling reactions: a modern strategy for C−C bond formation. *Chem. Soc. Rev.* **2011**, *40*, 5030−5048. (b) Wang, H.; Choi, I.; Rogge, T.; Kaplaneris, N.; Ackermann, L. Versatile and robust C−C activation by chelation-assisted manganese catalysis. *Nat. Catal.* **2018**, *1*, 993−1001. (c) Nogi, K.; Yorimitsu, H. Carbon−Carbon Bond Cleavage at Allylic Positions: Retro-allylation and Deallylation. *Chem. Rev.* **2021**, *121*, 345−364.

(8) Lutz, M. D. R.; Morandi, B. Metal-Catalyzed Carbon−Carbon Bond Cleavage of Unstrained Alcohols. *Chem. Rev.* **2021**, *121*, 300−326.

(9) (a) Urbanos, F.; Halcrow, M. A.; Fernandez-Baeza, J.; Dahan, F.; Labroue, D.; Chaudret, B. Selective Aromatization of the A-Ring of Steroids through C−C, C−H, and C−O Bond Activation by an Electrophilic Ruthenium Complex. *J. Am. Chem. Soc.* **1993**, *115*, 3484−3493. (b) Lv, X.-Y.; Abrams, R.; Martin, R. Copper-Catalyzed C(sp^3)-Amination of Ketone-Derived Dihydroquinazolinones by Aromatization-Driven C-C Bond Scission. *Angew. Chem., Int. Ed.* **2023**, *62*, No. e202217386.

(10) Xu, Y.; Qi, X.; Zheng, P.; Berti, C. C.; Liu, P.; Dong, G. Deacylative transformations of ketones via aromatization-promoted C−C bond activation. *Nature* **2019**, *567*, 373−378.

(11) (a) Chen, P.-h.; Billett, B. A.; Tsukamoto, T.; Dong, G. "Cut and Sew" Transformations via Transition-Metal-Catalyzed Carbon−Carbon Bond Activation. *ACS Catal.* **2017**, *7*, 1340−1360. (b) Sun, T.; Zhang, Y.; Qiu, B.; Wang, Y.; Qin, Y.; Dong, G.; Xu, T. Rhodium(I)-Catalyzed Carboacylation/Aromatization Cascade Initiated by Regioselective C−C Activation of Benzocyclobutenones. *Angew. Chem., Int. Ed.* **2018**, *57*, 2859−2863. (c) Deng, L.; Jin, L.; Dong, G. Fused-Ring Formation by an Intramolecular "Cut-and-Sew" Reaction between Cyclobutanones and Alkynes. *Angew. Chem., Int. Ed.* **2018**, *57*, 2702−2706. (d) Xia, Y.; Ochi, S.; Dong, G. Two-Carbon Ring Expansion of 1-Indanones via Insertion of Ethylene into Carbon−Carbon Bonds. *J. Am. Chem. Soc.* **2019**, *141*, 13038−13042.

(12) Ye, J.; Shi, Z.; Sperger, T.; Yasukawa, Y.; Kingston, C.; Schoenebeck, F.; Lautens, M. Remote C−H alkylation and C−C bond cleavage enabled by an in situ generated palladacycle. *Nat. Chem.* **2017**, *9*, 361−368.

(13) Yu, X.-Y.; Chen, J.-R.; Xiao, W.-J. Visible Light-Driven Radical-Mediated C−C Bond Cleavage/Functionalization in Organic Synthesis. *Chem. Rev.* **2021**, *121*, 506−561.

(14) Woo, J.; Christian, A. H.; Burgess, S. A.; Jiang, Y.; Mansoor, U. F.; Levin, M. D. Scaffold hopping by net photochemical carbon deletion of azaarenes. *Science* **2022**, *376*, 527−532.
(15) (a) McDonald, T. R.; Mills, L. R.; West, M. S.; Rousseaux, S. A. L. Selective Carbon−Carbon Bond Cleavage of Cyclopropanols. *Chem. Rev.* **2021**, *121*, 3−79. (b) Zhu, J.; Wang, J.; Dong, G. Catalytic activation of unstrained C(aryl)−C(aryl) bonds in 2,2′-biphenols. *Nat. Chem.* **2019**, *11*, 45−51. (c) Zhu, J.; Xue, Y.; Zhang, R.; Ratchford, B. L.; Dong, G. Catalytic Activation of Unstrained C(Aryl)−C(Alkyl) Bonds in 2,2′-Methylenediphenols. *J. Am. Chem. Soc.* **2022**, *144*, 3242−3249.
(16) (a) Arachchige, P. T. K.; Handunneththige, S.; Talipov, M. R.; Kalutharage, N.; Yi, C. S. Scope and Mechanism of the Redox-Active 1,2-Benzoquinone Enabled Ruthenium-Catalyzed Deaminative α-Alkylation of Ketones with Amines. *ACS Catal.* **2021**, *11*, 13962−13972. (b) Gnyawali, K.; Arachchige, P. T. K.; Yi, C. S. Synthesis of Flavanone and Quinazolinone Derivatives from the Ruthenium-Catalyzed Deaminative Coupling Reaction of 2'-Hydroxyaryl Ketones and 2-Aminobenzamides with Simple Amines. *Org. Lett.* **2022**, *24*, 218−222.
(17) Pannilawithana, N.; Yi, C. S. Catalytic Carbon−Carbon Bond Activation of Saturated and Unsaturated Carbonyl Compounds via Chelate-Assisted Coupling Reaction with Indoles. *ACS Catal.* **2020**, *10*, 5852−5861.
(18) (a) Ketcham, J. M.; Shin, I.; Montgomery, T. P.; Krische, M. J. Catalytic Enantioselective C−H Functionalization of Alcohols by Redox-Triggered Carbonyl Addition: Borrowing Hydrogen, Returning Carbon. *Angew. Chem., Int. Ed.* **2014**, *53*, 9142−9150. (b) Corma, A.; Navas, J.; Sabater, M. J. Advances in One-Pot Synthesis through Borrowing Hydrogen Catalysis. *Chem. Rev.* **2018**, *118*, 1410−1459.
(19) (a) Singleton, D. A.; Thomas, A. A. High-Precision Simultaneous Determination of Multiple Small Kinetic Isotope Effects at Natural Abundance. *J. Am. Chem. Soc.* **1995**, *117*, 9357−9358. (b) Frantz, D. E.; Singleton, D. A.; Snyder, J. P. ^{13}C Kinetic Isotope Effects for the Addition of Lithium Dibutylcuprate to Cyclohexenone. Reductive Elimination Is Rate-Determining. *J. Am. Chem. Soc.* **1997**, *119*, 3383−3384. (c) Nowlan, D. T.; Gregg, T. M.; Davies, H. M. L.; Singleton, D. A. Isotope Effects and the Nature of Selectivity in Rhodium-Catalyzed Cyclopropanations. *J. Am. Chem. Soc.* **2003**, *125*, 15902−15911.
(20) Perdew, J. P.; Burke, K.; Ernzerhof, M. Generalized Gradient Approximation Made Simple. *Phys. Rev. Lett.* **1996**, *77*, 3865−3868.
(21) Knizia, G.; Klein, J. E. M. N. Electron Flow in Reaction Mechanisms-Revealed from First Principles. *Angew. Chem., Int. Ed.* **2015**, *54*, 5518−5522.
(22) (a) Sierra, M. A.; Fernández, I.; Mancheño, M. J.; Gómez-Gallego, M.; Torres, M. R.; Cossío, F. P.; Arrieta, A.; Lecea, B.; Poveda, A.; Jiménez-Barbero, J. Light-Induced Aminocarbene to Imine Dyotropic Rearrangement in a Chromium (0) Center: An Unprecedented Reaction Pathway. *J. Am. Chem. Soc.* **2003**, *125*, 9572−9573. (b) Fernández, I.; Cossío, F. P.; Sierra, M. A. Photochemistry of Group 6 Fischer Carbene Complexes: Beyond the Photocarbonylation Reaction. *Acc. Chem. Res.* **2011**, *44*, 479−490.
(23) Hanwell, M. D.; Curtis, D. E.; Lonie, D. C.; Vandermeersch, T.; Zurek, E.; Hutchison, G. R. Avogadro: An Advanced Semantic Chemical Editor, Visualization, and Analysis Platform. *J. Cheminform.* **2012**, *4*, 17.
(24) Neese, F. The ORCA Program System. *Wiley Interdiscip. Rev. Comput. Mol. Sci.* **2012**, *2*, 73−78.
(25) Perdew, J. P.; Burke, K.; Ernzerhof, M. Generalized Gradient Approximation Made Simple. *Phys. Rev. Lett.* **1996**, *77*, 3865−3868.
(26) Caldeweyher, E.; Bannwarth, C.; Grimme, S. Extension of the D3 Dispersion Coefficient Model. *J. Chem. Phys.* **2017**, *147*, 034112.
(27) Weigend, F.; Ahlrichs, R. Balanced Basis Sets of Split Valence, Triple Zeta Valence and Quadruple Zeta Valence Quality for H to Rn: Design and Assessment of Accuracy. *Phys. Chem. Chem. Phys.* **2005**, *7*, 3297−3305.
(28) Zheng, J.; Xu, X.; Truhlar, D. G. Minimally Augmented Karlsruhe Basis Sets. *Theor. Chem. Acc.* **2011**, *128*, 295−305.
(29) Knizia, G. Intrinsic Atomic Orbitals: An Unbiased Bridge between Quantum Theory and Chemical Concepts. *J. Chem. Theory Comput.* **2013**, *9*, 4834−4843.
(30) Marenich, A. V.; Cramer, C. J.; Truhlar, D. G. Universal Solvation Model Based on Solute Electron Density and on a Continuum Model of the Solvent Defined by the Bulk Dielectric Constant and Atomic Surface Tensions. *J. Phys. Chem. B* **2009**, *113*, 6378−6396.

https://doi.org/10.1021/acs.organomet.3c00321
Organometallics 2023, 42, 2867−2880